energies

MDPI

Article

Simulation-Based Sizing of a Secondary Loop Cooling System for a Refrigerated Vehicle

Maximilian Lösch *, Markus Fallmann, Agnes Poks and Martin Kozek

Institute of Mechanics and Mechatronics, TU Wien, Getreidemarkt 9, 1060 Vienna, Austria; markus.fallmann@tuwien.ac.at (M.F.); agnes.poks@tuwien.ac.at (A.P.); martin.kozek@tuwien.ac.at (M.K.)
* Correspondence: maximilian.loesch@tuwien.ac.at; Tel.: +43-1-58801-325543

Abstract: Refrigerated transport by road is essential for the food industry but also contributes significantly to global energy consumption. In particular, last-mile transport, where the doors of the cooling chamber are opened frequently, puts a strain on energy efficiency and temperature control due to the high heat ingress from outside into the cooling chamber. These difficulties can be reduced by thermal energy storage systems, such as secondary loop refrigeration systems, if combined with a sophisticated control scheme. Although the storage capacity of such systems is critical for the overall performance of the cooling system, little research was performed regarding the sizing of the secondary loop thermal storage capacity. Therefore, this article examines the effect of the secondary loop thermal storage capacity on energy consumption and controller performance utilizing closed-loop simulations of a refrigerated vehicle model. Both a mixed-integer model predictive control scheme that can anticipate door openings and a conventional temperature controller are analyzed. An optimal thermal storage capacity of the secondary loop is found with the model predictive controller, whereas the conventional controller cannot exploit the secondary loop and thus shows significantly inferior performance. By using a dimensionless parameter for the thermal storage capacity of the secondary loop, the optimum found can be easily applied to refrigerated vehicles with various cooling chamber dimensions.

Keywords: refrigerated vehicle; secondary refrigerant; door openings; model predictive control; sizing

Citation: Lösch, M.; Fallmann, M.; Poks, A.; Kozek, M. Simulation-Based Sizing of a Secondary Loop Cooling System for a Refrigerated Vehicle. *Energies* **2023**, *16*, 6459. https://doi.org/10.3390/en16186459

Academic Editors: Ciro Aprea, Adrián Mota Babiloni, Rodrigo Llopis, Jaka Tušek, Angelo Maiorino, Andrej Žerovnik and Juan Manuel Belman-Flores

Received: 11 August 2023
Revised: 30 August 2023
Accepted: 4 September 2023
Published: 6 September 2023

1. Introduction

Approximately 8% of the worldwide electric energy consumption is caused by the food industry for refrigeration and maintaining the cold chain [1]. Much of this is attributable to refrigerated transport by road, whose cooling units are generally exposed to harsher conditions and have much poorer energy efficiency than stationary refrigeration units [2]. Therefore, for both economic and environmental reasons, substantial efforts are devoted to reducing the energy consumption of refrigerated vehicles [2–4]. However, the energy efficiency of refrigerated vehicles is still compromised by improper temperature control concepts, such as commonly used heuristic controllers. This is particularly evident for last-mile transport, where frequent door openings and the resulting heat ingress from the outside stress temperature control due to the high cooling demand required to cool down the cooling chamber after the door is closed [5].

Already in the design stage, the correct dimensioning of the individual components of the refrigerated vehicle is of great importance. For example, Maiorino et al. [6] studied the optimal design of the battery and photovoltaic panels of a hybrid refrigerated van. However, particular attention should be paid to the sizing of the cooling system, as this is one of the most critical components in terms of energy consumption and meeting the vehicle's cooling needs. Generally, refrigeration units are oversized for steady-state operation due to sizing for peak cooling loads [7,8], leading to increased energy consumption, wear of the compressor, and acquisition costs. In the literature, the sizing of the cooling equipment in

stationary conditions is broadly discussed, e.g., for HVAC systems in buildings [9,10] and a refrigeration system in an industrial plant [11]. Although already some simulation-based design methods for optimizing refrigeration systems exist [12–14], little has been done regarding the sizing of the cooling equipment of small-scale refrigerated vehicles with the consideration of door openings.

Therefore, this work analyzes the sizing of a secondary loop refrigeration unit for a small-scale refrigerated vehicle together with a mixed-integer model predictive controller (MPC). For this purpose, closed-loop simulations of a refrigerated vehicle with differently sized thermal energy storage (TES) capacities of the secondary loop are conducted. In the simulations, the system is disturbed by multiple door openings. Furthermore, the same simulations are performed using a rule-based proportional–integral (PI) controller, commonly used in industry for temperature control of refrigerated vehicles [15]. The two controllers and the differently sized secondary loops are compared based on their energy consumption and time required to bring the cooling chamber temperature back to the reference after door openings.

The use of TES has already found application in many fields [16], and it has been shown that they can significantly increase the efficiency of energy systems, e.g., photovoltaic panels [17]. TES systems are also very promising in the cold chain industry [18]. Cold TES can either use latent heat mediums like phase change materials (PCM) or sensible heat mediums. Storage systems with latent heat mediums generally have a much higher energy density than systems with sensible heat mediums, while TES systems using sensible heat mediums are more straightforward to realize, require less maintenance, and are less expensive [16], making them more suitable for small-scale refrigerated vehicles. In [19], the parameters of a PCM-based TES in a refrigerator cycle are analyzed. The results show that a suitably sized TES can significantly improve the cooling system's efficiency compared with a system without a TES. However, the analysis only included the cooling unit with the TES, without any cooling chamber. Jeong et al. [20] proposed a cooling system that stores low-temperature liquid refrigerant by actively controlling the refrigerant mass flow rate for the evaporator. Experimental results show that this allows the cooling capacity to be temporarily increased for peak cooling demand, thereby allowing a smaller cooling unit design.

Refrigeration systems with TES are especially beneficial for small-scale refrigerated vehicles, which often face door openings, resulting in high peak cooling demand [5]. Systems for road refrigeration can solely be based on TES, which are charged at the base, or be combined with a conventional cooling unit [3]. Mousazade et al. [21] studied the thermal performance of a cooling system with only a TES for a 6-ton refrigerated truck. In their experimental evaluation of three different PCM materials, the cooling chamber of a stationary truck could be kept solely by the TES at a constant temperature for a maximum of 5.1 h. However, cooling systems solely relying on a TES have a relatively high mass and practically no setpoint change capability. The storage capacity of PCM-based TES operated in parallel with a conventional cooling unit is analyzed in [14]. The influence of the sizing is given by means of closed-loop simulations with a heuristic control concept, although door openings were not taken into account. Shafiei et al. [22] used a similar cooling system architecture for their control concept for a refrigerated truck, which can achieve considerable energy savings by future load predictions and utilizing the TES. This paper also shows that only a suitable control structure can unleash the full potential of such combined systems, but their control concept lacks the inclusion of door openings.

Due to the high global warming potential of HFC refrigerants, increasingly more environmentally friendly liquids are being used as refrigerants, such as propane, ammonia, or hydrocarbon, which have the major drawback of being flammable. As a result, alternative refrigeration technologies, such as secondary loop refrigeration systems [23], are becoming more popular for physically separating hazardous refrigerants from the cooling chamber by adding an additional loop to the primary cooling cycle. Both single-phase (e.g., glycol mixtures and hybrid nanofluids [24]) and two-phase fluids (e.g., CO_2 [25], paraffin

emulsion [26], and salt hydrates [27]) are used as secondary refrigerants. Advantages of this architecture are reduced primary refrigerant charge and leakage and the ability to use the secondary loop as a TES [23]. Storage management of the TES allows a more flexible operation of the refrigeration unit without limiting the cooling of the cooling chamber, which means that the refrigeration unit can be operated generally more energy efficiently.

Due to the aforementioned reasons, TES systems with sensitive heat mediums are better suited for small-scale refrigerated vehicles. Therefore, this work considers a secondary loop cooling system with a glycol mixture as the secondary refrigerant, which is always kept above its freezing point. The modeling of a refrigerated vehicle with such a cooling system is described by Fallmann et al. [28]. In their work, a dynamic low-order model was estimated by a gray-box modeling approach using measurement data from a small-scale refrigerated vehicle with door openings. Based on that work, a control concept that takes advantage of the storage capability of the secondary loop was proposed and evaluated on a test bed in [29]. The experimental results show significant performance benefits regarding both energy consumption and peak cooling capacity for cooling after door openings. However, in the literature, the sizing of the secondary loop storage capacity was not studied until now.

The remainder of the paper is structured as follows: First, Section 2 describes the model of the small-scale refrigerated vehicle with a secondary loop cooling unit. Next, Section 3 explains the variation of the secondary loop storage capacity in the model. The two controllers to regulate the temperature inside the cooling chamber are introduced in Section 4. Section 5 summarizes the parameters of the simulation study, followed by the results in Section 6. The paper concludes with a discussion and conclusion in Section 7 and Section 8, respectively.

2. Model Description

For modeling the cooling chamber and the cooling unit of the small-scale refrigerated vehicle, the model proposed by Fallmann et al. [28] was adopted since it shows good agreement with measurement data from a real-world refrigerated vehicle. The only modification to the original model was the removal of the heater acting as a disturbance heat flow in the cooling chamber, as this disturbance is irrelevant to this work. In the following, a brief overview of the model is given, and the interested reader is referred to [28], where the modeling of the system and its validation is explained elaborately. Note that the thermodynamic quantities in this work correspond to ISO 80000-5:2019 [30].

Figure 1 shows the system scheme with the cooling unit and cooling chamber, as well as important modeling variables. The cooling unit is a commercially available secondary loop refrigeration unit [31], which can be divided into a cooling loop and a storage loop. The cooling unit can be switched on and off by $s_{\mathrm{cu}} \in \{0,1\}$, activating/deactivating the compressor of the cooling loop, the condenser fan, and the glycol pump of the storage loop. The cooling loop is a standard vapor compression refrigeration cycle with propane as refrigerant, powered by a compressor rotating with the speed $n_{\mathrm{cpr}} \in \mathbb{R}$. The storage loop, containing glycol, can store thermal energy supplied by the cooling loop and release thermal energy to the air in the cooling chamber through an air chiller. The glycol temperatures at the inflowing and outflowing position of the air chiller are given by $\vartheta_{\mathrm{gly}}^{\mathrm{in}} \in \mathbb{R}$ and $\vartheta_{\mathrm{gly}}^{\mathrm{out}} \in \mathbb{R}$, respectively. A fan mounted to the air chiller evokes a heat flow, $\dot{Q}_{\mathrm{ac}} \in \mathbb{R}$, either due to natural or forced convection between the secondary loop and the air inside the cooling chambers, depending on the status of the fan $s_{\mathrm{acf}} \in \{0,1\}$. The interior of the cooling chamber, with the lumped air temperature $\vartheta_{\mathrm{cc}} \in \mathbb{R}$, is separated from the environment by insulated walls and a door. A second-order system describes the heat transfer characteristics of the insulated walls with the two wall temperatures $\vartheta_{\mathrm{w},1} \in \mathbb{R}$ and $\vartheta_{\mathrm{w},2} \in \mathbb{R}$. Door openings are indicated by $s_{\mathrm{door}} \in \{0,1\}$, which entails a heat flow between the air inside the cooling chamber and the ambient air (ambient air temperature $\vartheta_{\mathrm{amb}} \in \mathbb{R}$). Furthermore, the model describes the power consumption of the compressor $P_{\mathrm{cpr}} \in \mathbb{R}$, the condenser

fan $P_{cf} \in \mathbb{R}$, the glycol pump $P_p \in \mathbb{R}$, the air chiller fan $P_{acf} \in \mathbb{R}$, and the total consumption of all components $P_{tot} \in \mathbb{R}$.

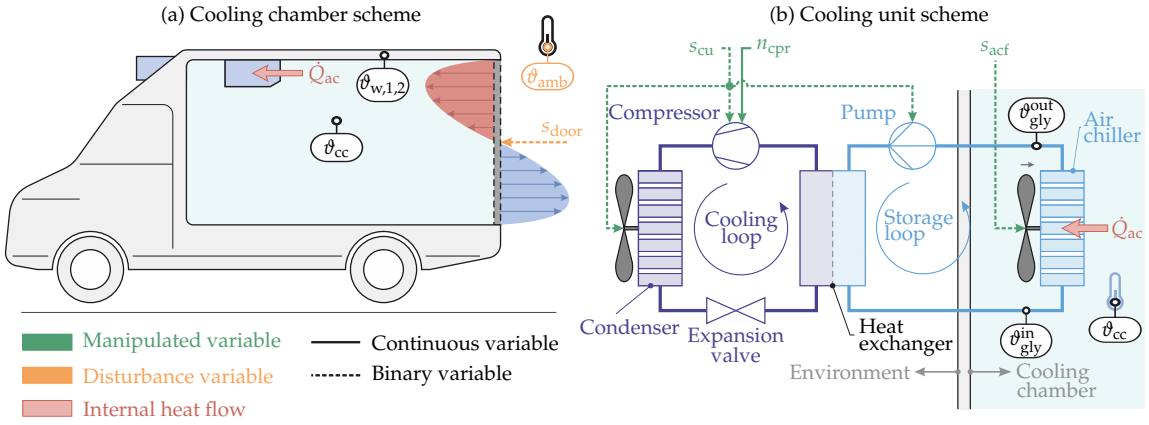

Figure 1. Schematic illustration of the refrigerated vehicle, consisting of a cooling chamber (**a**) and a secondary loop cooling unit (**b**). Important temperatures ϑ, the air chiller heat flow $\dot{Q}_{ac}$, switching variables s, and the compressor speed n_{cpr} are highlighted. Door openings are indicated by the warm inflowing air colored in red and the outflowing cold air colored in blue. The secondary loop refrigeration unit can be divided into a cooling loop with propane as refrigerant and a storage loop filled with a glycol mixture. Figure adopted from [28].

The mathematical description of the dynamic model relies on first principles, which is explained comprehensively in [28]. Given that the model comprises both continuous and binary variables, it is a hybrid model [32]. Hence, a model formulation with a mode selector and a switched affine system is chosen. This approach allows to separate binary and continuous variables. The mode selector maps the three binary variables of the model on one of the eight modes $m \in \{1, 2, \ldots, 8\}$, see Table 1.

Table 1. Classification of the mode m depending on the status of the cooling unit s_{cu}, the air chiller fan s_{acf}, and the door s_{door}.

Mode $m(t)$	$s_{cu}(t)$	$s_{acf}(t)$	$s_{door}(t)$
1	0	0	0
2	0	0	1
3	0	1	0
4	0	1	1
5	1	0	0
6	1	0	1
7	1	1	0
8	1	1	1

Depending on the mode, an associated affine model is selected in the switched affine system. This model comprises solely continuous variables and can be written in state-space formulation as

$$\dot{\boldsymbol{x}}_c(t;m) = \boldsymbol{A}(m)\,\boldsymbol{x}_c(t;m) + \boldsymbol{B}(m)\,u_c(t) + \boldsymbol{E}(m)\,v_c(t) + \boldsymbol{g}(m), \tag{1}$$

$$\boldsymbol{y}_c(t;m) = \boldsymbol{C}(m)\,\boldsymbol{x}_c(t;m) + \boldsymbol{D}(m)\,u_c(t) + \boldsymbol{F}(m)\,v_c(t) + \boldsymbol{h}(m), \tag{2}$$

where $t \in \mathbb{R}_{\geq 0}$ denotes the continuous time. This state-space model describes the system dynamics by transforming the state vector $\boldsymbol{x}_c \in \mathbb{R}^4$ according to

$$\boldsymbol{x}_{\mathrm{c}}(t;m) := \begin{bmatrix} \vartheta_{\mathrm{cc}}(t;m) \\ \vartheta^{\mathrm{out}}_{\mathrm{gly}}(t;m) \\ \vartheta_{\mathrm{w},1}(t;m) \\ \vartheta_{\mathrm{w},2}(t;m) \end{bmatrix} \tag{3}$$

with the continuous input $u_{\mathrm{c}} \in \mathbb{R}$ and disturbance $v_{\mathrm{c}} \in \mathbb{R}$ given by $u_{\mathrm{c}}(t) := n_{\mathrm{cpr}}(t)$ and $v_{\mathrm{c}}(t) := \vartheta_{\mathrm{amb}}(t)$, respectively, into the model outputs $\boldsymbol{y}_{\mathrm{c}} \in \mathbb{R}^8$ according to

$$\boldsymbol{y}_{\mathrm{c}}(t;m) := \begin{bmatrix} \vartheta_{\mathrm{cc}}(t;m) \\ \vartheta^{\mathrm{in}}_{\mathrm{gly}}(t;m) \\ \vartheta^{\mathrm{out}}_{\mathrm{gly}}(t;m) \\ P_{\mathrm{tot}}(t;m) \\ P_{\mathrm{cpr}}(t;m) \\ P_{\mathrm{cf}}(m) \\ P_{\mathrm{p}}(m) \\ P_{\mathrm{acf}}(m) \end{bmatrix}. \tag{4}$$

The transformation is defined by the system matrix $\boldsymbol{A} \in \mathbb{R}^{4\times4}$, input vector $\boldsymbol{B} \in \mathbb{R}^4$, system disturbance vector $\boldsymbol{E} \in \mathbb{R}^4$, affine system vector $\boldsymbol{g} \in \mathbb{R}^4$, output matrix $\boldsymbol{C} \in \mathbb{R}^{8\times4}$, feedthrough vector $\boldsymbol{D} \in \mathbb{R}^8$, output disturbance vector $\boldsymbol{F} \in \mathbb{R}^8$, and affine output vector $\boldsymbol{h} \in \mathbb{R}^8$. The model matrices of the state space systems and their parameters were adopted from [28], where they were experimentally identified and validated. Their values are given in Appendix A.

3. Parameter Variation

To investigate different thermal capacities of the storage loop, the scaling factor $K^{\mathrm{scl}}_{\mathrm{sl}} \in \mathbb{R}_{\geq 0}$ is introduced. In the case of the unscaled model (see [28]), the dynamics of the glycol temperature are given by

$$\chi_3^{-1} \frac{d}{dt} \vartheta^{\mathrm{out}}_{\mathrm{gly}}(t;m) = \frac{\chi_2}{\chi_3} \left[\vartheta^{\mathrm{in}}_{\mathrm{gly}}(t;m) - \vartheta^{\mathrm{out}}_{\mathrm{gly}}(t;m) \right] + \dot{Q}_{\mathrm{ac}}(t;m) \tag{5}$$

with the model parameters $\chi_2 \in \mathbb{R}$ and $\chi_3 \in \mathbb{R}$. The thermal capacity of the glycol is defined by the ratio of the heat added to the rate of change of its temperature [33]. Hence, the thermal capacity of the glycol in the secondary loop is given by $C_{\mathrm{gly}} = \chi_3^{-1} \in \mathbb{R}$. By adapting Equation (5) according to

$$K^{\mathrm{scl}}_{\mathrm{sl}} C_{\mathrm{gly}} \frac{d}{dt} \vartheta^{\mathrm{out}}_{\mathrm{gly}}(t;m) = \frac{\chi_2}{\chi_3} \left[\vartheta^{\mathrm{in}}_{\mathrm{gly}}(t;m) - \vartheta^{\mathrm{out}}_{\mathrm{gly}}(t;m) \right] + \dot{Q}_{\mathrm{ac}}(t;m), \tag{6}$$

the thermal storage capacity of the glycol is scaled linearly by the factor $K^{\mathrm{scl}}_{\mathrm{sl}}$. With $K^{\mathrm{scl}}_{\mathrm{sl}} = 1$, the same storage capacity of the secondary loop as in the unscaled model is obtained. A scaling factor between 0 and 1 describes a secondary loop with lower thermal storage capacity, and a scaling factor greater than 1 represents a storage loop with higher storage capacity compared with the unscaled model. Later in this work, $K^{\mathrm{scl}}_{\mathrm{sl}}$ is varied to investigate the effects of this sizing parameter on the closed-loop performance of the refrigerated vehicle.

4. Temperature Control

Two different control concepts were evaluated for controlling the temperature inside the cooling chamber. One is an MPC, an advanced control algorithm based on an online optimization of the system. The other is a rule-based PI controller commonly used in industry for the temperature control of refrigerated vehicles. Both control schemes were adopted from [29] with small modifications and are explained in detail below.

4.1. Model Predictive Controller

The MPC calculates the control inputs based on minimizing an objective function subject to constraints over a finite prediction horizon with the length $N_{\mathrm{pr}} \in \mathbb{N}$. This optimization problem is schematized in Figure 2 to support the upcoming elaboration of the control scheme.

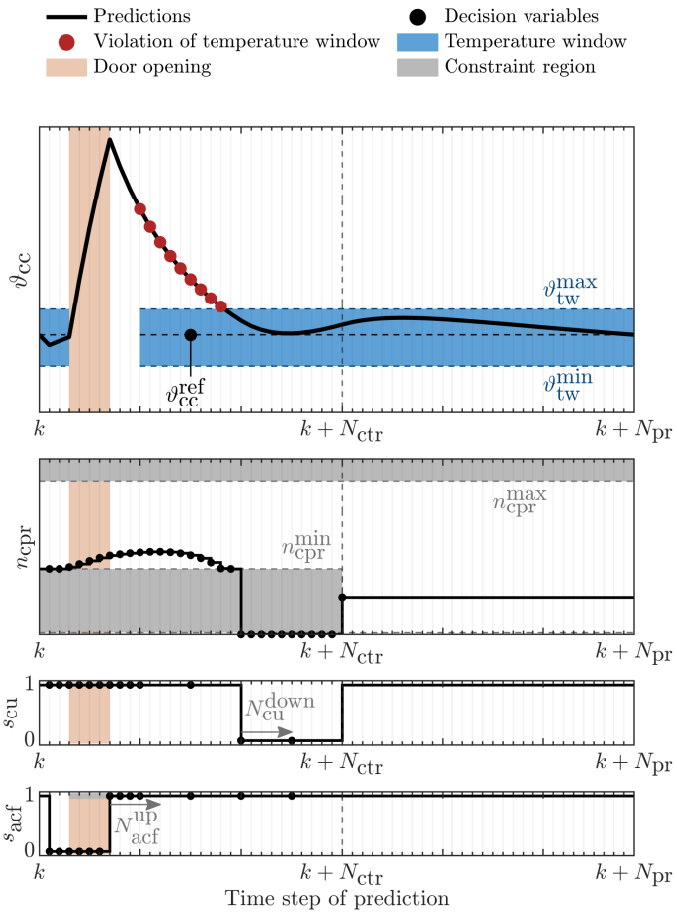

Figure 2. Illustration of the MPCs optimization problem with a future door opening, highlighted by an orange background shading. Decision variables and constraints are depicted schematically. A blue background shading highlights the temperature window, and deviations from that window are marked red. Figure adapted from [29].

Model-based predictions of the future trajectory of the system quantities are used to select the control inputs optimally in terms of the objective function. Therefore, the controller utilizes a discretized version of the state-space model derived in Section 2, using zero-order hold with sampling time T_{s}, yielding

$$\boldsymbol{x}_{\mathrm{c}}(k+1;m) = \boldsymbol{A}_{\mathrm{d}}(m)\,\boldsymbol{x}_{\mathrm{c}}(k;m) + \boldsymbol{B}_{\mathrm{d}}(m)\,u_{\mathrm{c}}(k) + \boldsymbol{E}_{\mathrm{d}}(m)\,v_{\mathrm{c}}(k) + \boldsymbol{g}_{\mathrm{d}}(m) \tag{7}$$

$$\boldsymbol{y}_{\mathrm{c}}(k;m) = \boldsymbol{C}_{\mathrm{d}}(m)\,\boldsymbol{x}_{\mathrm{c}}(k;m) + \boldsymbol{D}_{\mathrm{d}}(m)\,u_{\mathrm{c}}(k) + \boldsymbol{F}_{\mathrm{d}}(m)\,v_{\mathrm{c}}(k) + \boldsymbol{h}_{\mathrm{d}}(m) \tag{8}$$

with the current sampling instance $k \in \mathbb{N}$ and discretized model matrices $\boldsymbol{A}_{\mathrm{d}} \in \mathbb{R}^{4\times4}$, $\boldsymbol{B}_{\mathrm{d}} \in \mathbb{R}^{4}$, $\boldsymbol{E}_{\mathrm{d}} \in \mathbb{R}^{4}$, $\boldsymbol{g}_{\mathrm{d}} \in \mathbb{R}^{4}$, $\boldsymbol{C}_{\mathrm{d}} \in \mathbb{R}^{8\times4}$, $\boldsymbol{D}_{\mathrm{d}} \in \mathbb{R}^{8}$, $\boldsymbol{F}_{\mathrm{d}} \in \mathbb{R}^{8}$, and $\boldsymbol{h}_{\mathrm{d}} \in \mathbb{R}^{8}$ to compute the stacked vector of future states $\boldsymbol{X}_{\mathrm{c}} \in \mathbb{R}^{4\,N_{\mathrm{pr}}}$ and outputs $\boldsymbol{Y}_{\mathrm{c}} \in \mathbb{R}^{8\,N_{\mathrm{pr}}}$ at the current sampling instance k according to

$$\boldsymbol{X}_\mathrm{c} \coloneqq \begin{bmatrix} \boldsymbol{x}_\mathrm{c}(k+1|k;m) \\ \boldsymbol{x}_\mathrm{c}(k+2|k;m) \\ \vdots \\ \boldsymbol{x}_\mathrm{c}(k+N_\mathrm{pr}|k;m) \end{bmatrix}, \; \boldsymbol{Y}_\mathrm{c} \coloneqq \begin{bmatrix} \boldsymbol{y}_\mathrm{c}(k|k;m) \\ \boldsymbol{y}_\mathrm{c}(k+1|k;m) \\ \vdots \\ \boldsymbol{y}_\mathrm{c}(k+N_\mathrm{pr}-1|k;m) \end{bmatrix} \tag{9}$$

using the current state vector $\boldsymbol{x}(k;m)$, and the vectors of stacked future continuous inputs, binary inputs, continuous disturbances, and binary disturbances, $\boldsymbol{U}_\mathrm{c} \in \mathbb{R}^{N_\mathrm{pr}}$, $\boldsymbol{U}_\mathrm{b} \in \mathbb{R}^{2\,N_\mathrm{pr}}$, $\boldsymbol{V}_\mathrm{c} \in \mathbb{R}^{N_\mathrm{pr}}$, and $\boldsymbol{V}_\mathrm{b} \in \mathbb{R}^{N_\mathrm{pr}}$, respectively, see (10):

$$\begin{aligned} \boldsymbol{U}_\mathrm{c} &\coloneqq \begin{bmatrix} u_\mathrm{c}(k) \\ u_\mathrm{c}(k+1) \\ \vdots \\ u_\mathrm{c}(k+N_\mathrm{pr}-1) \end{bmatrix}, \; \boldsymbol{U}_\mathrm{b} \coloneqq \begin{bmatrix} \boldsymbol{u}_\mathrm{b}(k) \\ \boldsymbol{u}_\mathrm{b}(k+1) \\ \vdots \\ \boldsymbol{u}_\mathrm{b}(k+N_\mathrm{pr}-1) \end{bmatrix}, \\ \boldsymbol{V}_\mathrm{c} &\coloneqq \begin{bmatrix} v_\mathrm{c}(k) \\ v_\mathrm{c}(k+1) \\ \vdots \\ v_\mathrm{c}(k+N_\mathrm{pr}-1) \end{bmatrix}, \; \boldsymbol{V}_\mathrm{b} \coloneqq \begin{bmatrix} \boldsymbol{v}_\mathrm{b}(k) \\ \boldsymbol{v}_\mathrm{b}(k+1) \\ \vdots \\ \boldsymbol{v}_\mathrm{b}(k+N_\mathrm{pr}-1) \end{bmatrix} \end{aligned} \tag{10}$$

The vectors of future disturbances are based on ambient temperature and door status predictions. Furthermore, constraints to the optimization problem have to be observed to consider the system's physical limits and reduce the optimization problem's complexity to ease the computational effort required to solve it.

4.1.1. Constraints

To reduce the computational effort of the MPC, a control horizon $N_\mathrm{ctr} \in \mathbb{N}_{\leq N_\mathrm{pr}}$ is introduced. Only during the control horizon, the controller can select the inputs. For the rest of the prediction horizon, the inputs are constant. Door openings are excluded in that period to ensure that the controller can track a reference temperature after the control horizon. For the same reason, the cooling unit and the air chiller fan are active after the control horizon. These conditions imply the following constraints:

$$n_\mathrm{cpr}(k+i) = n_\mathrm{cpr}(k+N_\mathrm{ctr}), \qquad \forall i \in \{N_\mathrm{ctr}, N_\mathrm{ctr}+1, \ldots, N_\mathrm{pr}-1\} \tag{11}$$

$$s_\mathrm{cu}(k+i) = 1, \qquad \forall i \in \{N_\mathrm{ctr}, N_\mathrm{ctr}+1, \ldots, N_\mathrm{pr}-1\} \tag{12}$$

$$s_\mathrm{acf}(k+i) = 1, \qquad \forall i \in \{N_\mathrm{ctr}, N_\mathrm{ctr}+1, \ldots, N_\mathrm{pr}-1\} \tag{13}$$

$$s_\mathrm{door}(k+i) = 0, \qquad \forall i \in \{N_\mathrm{ctr}, N_\mathrm{ctr}+1, \ldots, N_\mathrm{pr}-1\} \tag{14}$$

Furthermore, the compressor is physically limited by a lower, $n_\mathrm{cpr}^\mathrm{min} \in \mathbb{R}$, and upper speed, $n_\mathrm{cpr}^\mathrm{max} \in \mathbb{R}$, when the cooling unit is active. When the cooling unit is inactive, the compressor speed is 0. Due to the enforced constant inputs after the control horizon N_ctr, it was necessary to soften the limits of the lower compressor speed after N_ctr to track the reference temperature during this part of the horizon:

$$n_\mathrm{cpr}(k+i) \leq n_\mathrm{cpr}^\mathrm{max}\, s_\mathrm{cu}(k+i), \quad i \in \{0, 1, \ldots, N_\mathrm{pr}-1\} \tag{15}$$

$$n_\mathrm{cpr}(k+i) \geq n_\mathrm{cpr}^\mathrm{min}\, s_\mathrm{cu}(k+i), \quad i \in \{0, 1, \ldots, N_\mathrm{ctr}-1\} \tag{16}$$

$$n_\mathrm{cpr}(k+i) \geq 0, \qquad i \in \{N_\mathrm{ctr}, N_\mathrm{ctr}+1, \ldots, N_\mathrm{pr}-1\} \tag{17}$$

However, the control inputs after the control horizon are never implemented on the plant due to the receding horizon control law, explained below, and thus, the actual physical limits of the plant are observed.

Since the secondary refrigerant should always be in a liquid state, the following constraints apply to the minimum glycol temperature:

$$\vartheta_{\text{gly}}^{\text{out}}(k+i|k;m) \geq \vartheta_{\text{gly}}^{\text{out,min}}, \qquad \forall i \in \{1, 2 \ldots N_{\text{pr}}\}, \tag{18}$$

where $\vartheta_{\text{gly}}^{\text{out,min}} \in \mathbb{R}$ is the freezing temperature of the glycol.

Additionally, the minimum up and down times are enforced on the cooling unit and air chiller fan to prohibit extensive switching, which can significantly reduce the lifespan of the components. The formulation of these constraints was taken from [34] according to

$$s_\mu(k+i) - s_\mu(k+i-1) \leq s_\mu(\tau_{\text{up}}), \qquad \forall i \in \left\{-N_\mu^{\text{up}}, -N_\mu^{\text{up}}+1, \ldots, N_{\text{ctr}}-1\right\} \tag{19}$$

$$s_\mu(k+i-1) - s_\mu(k+i) \leq 1 - s_\mu(\tau_{\text{down}}), \qquad \forall i \in \left\{-N_\mu^{\text{down}}, -N_\mu^{\text{down}}+1, \ldots, N_{\text{ctr}}-1\right\} \tag{20}$$

with $\tau_{\text{up}} \in \{k+i, k+i+1, \ldots, \min(k+N_{\text{ctr}}-1, k+i+N_\mu^{\text{up}}-1)\}$, $\tau_{\text{down}} \in \{k+i, k+i+1, \ldots, \min(k+N_{\text{ctr}}-1, k+i+N_\mu^{\text{down}}-1)\}$, and $\mu \in \{\text{cu,acf}\}$, where $N_\mu^{\text{up}} \in \mathbb{N}$ and $N_\mu^{\text{down}} \in \mathbb{N}$ is the minimum up and down time in samples, respectively.

The modes where the fan is active while the door is open are very disadvantageous in terms of energy efficiency due to the increased air exchange between the inside of the cooling chamber and the environment. However, these dynamics were not considered by [28] when modeling the system. Thus, the modes were generally prohibited in the control law of the MPC:

$$s_{\text{acf}}(k+i)\, s_{\text{door}}(k+i) = 0, \qquad \forall i \in \{0, 1 \ldots, N_{\text{pr}}-1\}. \tag{21}$$

The computational cost of solving optimization problems scales with the degree of freedom (i.e., number of free inputs), and binary decision variables place a particular burden on solving such problems. Therefore, move blocking constraints, similar to those described by [35], are introduced for the binary input variables. Instead of optimizing all the binary decision variables in the control horizon $\boldsymbol{U}_{\text{b,ctr}} := \left[\boldsymbol{u}_{\text{b}}^{\text{T}}(k), \boldsymbol{u}_{\text{b}}^{\text{T}}(k+1), \ldots, \boldsymbol{u}_{\text{b}}^{\text{T}}(k+N_{\text{ctr}}-1)\right]^{\text{T}} \in \mathbb{R}^{2(N_{\text{ctr}}-1)}$, the problem is restated in terms of finding the optimal reduced binary input vector $\boldsymbol{U}_{\text{b,ctr}}^{\text{red}} := \left[\boldsymbol{u}_{\text{b,1}}^{\text{red}}, \boldsymbol{u}_{\text{b,2}}^{\text{red}}, \ldots, \boldsymbol{u}_{\text{b,M}}^{\text{red}}\right]^{\text{T}} \in \mathbb{R}^{2M}$ with $M \in \mathbb{N}_{\leq (N_{\text{ctr}}-1)}$ binary decision vectors, which relates to $\boldsymbol{U}_{\text{b,ctr}}$ by:

$$\boldsymbol{U}_{\text{b,ctr}} := \left(\boldsymbol{T}_{\text{mb}} \otimes \boldsymbol{I}_2\right) \boldsymbol{U}_{\text{b,ctr}}^{\text{red}}, \tag{22}$$

where $\otimes$ denotes the Kronecker product and $\boldsymbol{T}_{\text{mb}} \in \mathbb{R}^{(N_{\text{ctr}}-1)\times M}$ is the blocking matrix, which contains only ones and zeros and has exactly one non-zero element in each row.

4.1.2. Objective Function

The objective function $J \in \mathbb{R}_{\geq 0}$ of the MPC can be divided into multiple terms according to

$$J := J_{\text{tw}} + J_{\text{con}} + J_{\Delta n_{\text{cpr}}} + J_{\text{t}}, \tag{23}$$

where $J_{\text{tw}} \in \mathbb{R}_{\geq 0}$ penalizes the violation of a prescribed temperature window, $J_{\text{con}} \in \mathbb{R}_{\geq 0}$ the power consumption over the horizon, $J_{\Delta n_{\text{cpr}}} \in \mathbb{R}_{\geq 0}$ the rate of change of the compressor speed from one sample to the next, and $J_{\text{t}} \in \mathbb{R}_{\geq 0}$ the final temperature at the end of the prediction horizon.

The MPC regulates the air temperature inside the cooling chamber to stay within a so-called temperature window with the lower bound $\vartheta_{\text{tw}}^{\text{min}} \in \mathbb{R}$ and the upper bound $\vartheta_{\text{tw}}^{\text{max}} \in \mathbb{R}$. However, this temperature window is not always active since door openings pose a major disturbance, making it infeasible to hold the cooling chamber temperature within the boundaries of the temperature window. Therefore, the temperature window is switched to be inactive by the variable $s_{\text{tw}} \in \{0, 1\}$ during and shortly after door openings. Hence, the profile of the temperature window status $\boldsymbol{S}_{\text{tw}} := \left[s_{\text{tw}}(k+1), s_{\text{tw}}(k+2), \ldots, s_{\text{tw}}(k+N_{\text{pr}})\right]^{\text{T}} \in \mathbb{R}^{N_{\text{pr}}}$ is closely coupled to the predicted door openings and is also given as input to the opti-

mization problem. In the objective function, a deviation from the temperature window is penalized in each sample by the factor $Q \in \mathbb{R}_{\geq 0}$ according to

$$J_{\mathrm{tw}} := Q \sum_{i=1}^{N_{\mathrm{pr}}} \delta_{\mathrm{tw}}(k+i|k)\, s_{\mathrm{tw}}(k+i) \tag{24}$$

with the helper variable $\delta_{\mathrm{tw}} \in \{0,1\}$, indicating a violation of the temperature window given by

$$\delta_{\mathrm{tw}}(k+i|k;m) := \begin{cases} 1, & \text{if } \vartheta_{\mathrm{tw}}^{\max} \leq \vartheta_{\mathrm{cc}}(k+i|k;m) \leq \vartheta_{\mathrm{tw}}^{\min} \\ 0, & \text{otherwise} \end{cases}. \tag{25}$$

In addition, the controller should minimize energy consumption. Therefore, the total power consumption in each time step is penalized by the factor $R_1 \in \mathbb{R}_{\geq 0}$, according to

$$J_{\mathrm{con}} := R_1 \sum_{i=1}^{N_{\mathrm{pr}}-1} P_{\mathrm{tot}}(k+i). \tag{26}$$

To limit fast changes in the compressor speed, which could damage the components of the refrigeration system, the quadratic rate of change of the compressor speed is weighted by the factor $R_2 \in \mathbb{R}_{\geq 0}$ according to

$$J_{\Delta n_{\mathrm{cpr}}} := R_2 \sum_{i=1}^{N_{\mathrm{pr}}-1} \left[n_{\mathrm{cpr}}(k+i) - n_{\mathrm{cpr}}(k+i-1) \right]^2. \tag{27}$$

At the end of the prediction horizon, the terminal cost is added to the objective function, given by

$$J_{\mathrm{t}} := T_1\, \delta_{\mathrm{t}}(k+N_{\mathrm{pr}}|k;m) + \delta_{\mathrm{t}}(k+N_{\mathrm{pr}}|k;m)\, T_2\, \delta_{\mathrm{t}}(k+N_{\mathrm{pr}}|k;m) \tag{28}$$

with the factors $T_1 \in \mathbb{R}_{\geq 0}$ and $T_2 \in \mathbb{R}_{\geq 0}$ weighting the linear and quadratic deviations from the reference temperature $\vartheta_{\mathrm{cc}}^{\mathrm{ref}} \in \mathbb{R}$ at the last time step of the prediction horizon, and the helper variable $\delta_{\mathrm{t}} \in \mathbb{R}_{\geq 0}$ indicating the temperature deviation at the end of N_{pr} according to

$$\delta_{\mathrm{t}}(k+N_{\mathrm{pr}}|k;m) = \left| \vartheta_{\mathrm{cc}}(k+N_{\mathrm{pr}}|k;m) - \vartheta_{\mathrm{cc}}^{\mathrm{ref}} \right|. \tag{29}$$

4.1.3. Implementation

With the objective function and all constraints defined, the optimization problem of the MPC can be stated according to

$$\left[\boldsymbol{u}_{\mathrm{b,ctr}}^{\mathrm{red},*}, \boldsymbol{u}_{\mathrm{c}}^{*} \right] = \underset{\boldsymbol{u}_{\mathrm{b,ctr}}^{\mathrm{red}}, \boldsymbol{u}_{\mathrm{c}}}{\arg\min}\, J \tag{30}$$

subject to (7)–(8) and (11)–(22) with * indicating the optimized control variables. Considering that the optimization problem comprises discrete and continuous variables, the controller is a mixed-integer MPC [32]. Compared to a conventional MPC with only continuous variables, a mixed-integer MPC can explicitly consider the switching dynamics of the model, e.g., induced by door openings, and thus improve the accuracy of the controller's predictions. The optimization problem of the MPC is solved at each time step, with only the first set of optimized inputs implemented on the system, resulting in a receding horizon control law.

Standard guidelines [29,36] were used to obtain the MPCs parameters. Care was taken to keep the computational complexity within limits and obtain a controller performance close to the global optimality. The model's fastest eigenvalues determine the controller's maximum sampling time T_{s} according to the Nyquist criterion. At the same time, the slowest dynamics dictate the minimum length of the prediction horizon N_{pr}. Extensive

closed-loop simulations were performed to select the control horizon and move blocking constraints to reduce the computational complexity of the controller while preserving the global optimality. In Table 2, the parameters of the MPC are listed. The optimization problem is constructed using the Matlab framework Yalmip [37] and solved using the Gurobi solver [38].

Table 2. MPC parameters.

Parameter	Value
T_s	20 s
N_pr	60
N_ctr	31
$n_\mathrm{cpr}^\mathrm{min}$	700 rpm
$n_\mathrm{cpr}^\mathrm{max}$	5000 rpm
$\vartheta_\mathrm{gly}^\mathrm{out,min}$	−35 °C
$N_\mu^\mathrm{up}, N_\mu^\mathrm{down}$	5
T_mb	see Appendix B
M	13
$\vartheta_\mathrm{cc}^\mathrm{ref}$	5 °C
$\vartheta_\mathrm{tw}^\mathrm{min}$	4.5 °C
$\vartheta_\mathrm{tw}^\mathrm{max}$	5.5 °C
Q	$8 \cdot 10^6$
R_1	0.1
R_2	$1 \cdot 10^{-5}$
T_1	$5 \cdot 10^3$
T_2	$1 \cdot 10^3$

4.2. Rule-Based PI Controller

With this control scheme, the refrigeration unit is operated based on a PI control law to track the reference temperature $\vartheta_\mathrm{cc}^\mathrm{ref}$. However, the physical limits of the compressor speed and the two binary control variables necessitate additional rules to track the reference temperature and compute the binary variables. In Figure 3, the calculation of the status of the cooling unit and fan are visualized, supporting the upcoming elaboration.

For the sake of simplicity, the two binary manipulated variables are operated in parallel, yielding the condition

$$s_\mathrm{cu}(k) = s_\mathrm{acf}(k) = s_\mu(k) \tag{31}$$

As with the MPC, rules for the minimum up and down times are enforced. By operating the air chiller fan and cooling unit in parallel, a uniform minimum up and down time, $N^\mathrm{up} \in \mathbb{N}$ and $N^\mathrm{down} \in \mathbb{N}$, can be defined according to

$$N^\mathrm{up} = \max\left(N_\mathrm{cu}^\mathrm{up}, N_\mathrm{acf}^\mathrm{up}\right) \tag{32}$$

$$N^\mathrm{down} = \max\left(N_\mathrm{cu}^\mathrm{down}, N_\mathrm{acf}^\mathrm{down}\right). \tag{33}$$

The air chiller fan becomes inactive when the door opens since this is, as described above, a very inefficient operating mode. Hence, the cooling unit is also set to be inactive due to the parallel operation.

If none of the above cases apply, an on–off controller computes the binary control variables with the following control law:

$$s_\mu(k) = \begin{cases} 1, & \text{if } e(k) \leq -H_\vartheta \\ 0, & \text{if } e(k) \geq H_\vartheta \\ s_\mu(k-1) & \text{otherwise} \end{cases}, \tag{34}$$

where $e(k) := \vartheta_{\mathrm{cc}}^{\mathrm{ref}} - \vartheta_{\mathrm{cc}}(k) \in \mathbb{R}$ is the control error and $H_\vartheta \in \mathbb{R}_{\geq 0}$ is the switching threshold.

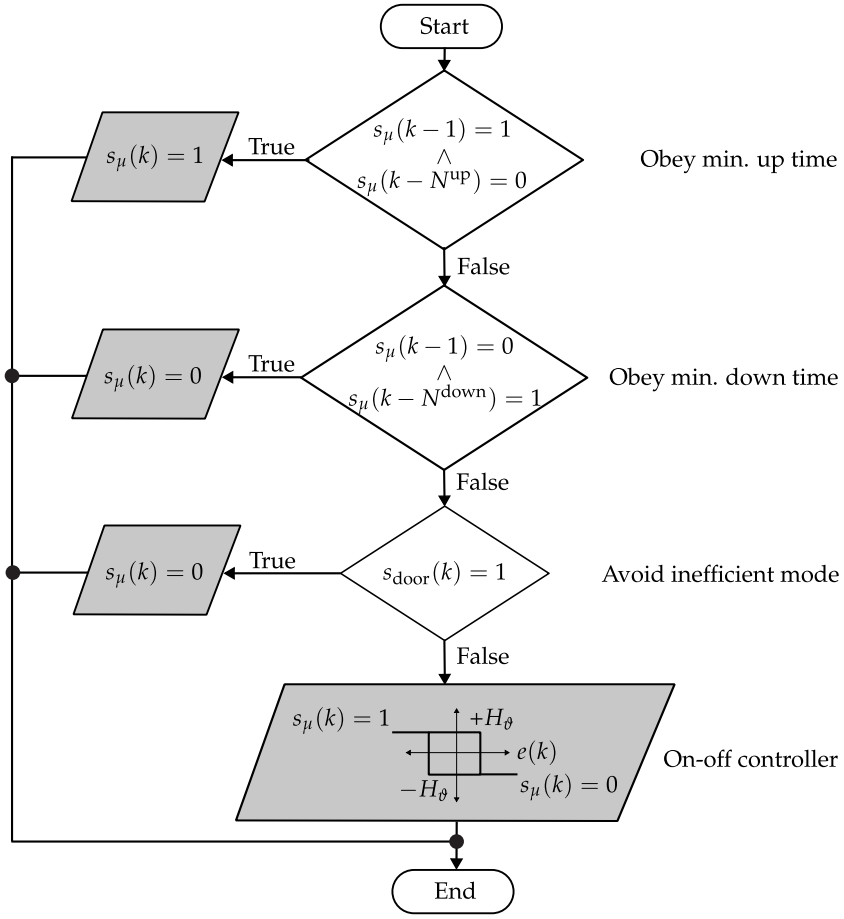

Figure 3. Flow diagram for the calculation of the binary control variables s_μ with $\mu \in \{\mathrm{cu,acf}\}$.

The compressor speed is 0 when the cooling unit is inactive. Otherwise, the speed is determined based on the discrete-time PI control law [39] according to

$$n_{\mathrm{cpr}}(k) = n_{\mathrm{cpr}}(k-1) + P_{\mathrm{PI}}\, e(k) + \left[T_{\mathrm{s}}\ I_{\mathrm{PI}} - P_{\mathrm{PI}}\right]\ e(k-1) \tag{35}$$

with the proportional gain $P_{\mathrm{PI}} \in \mathbb{R}$ and the integral gain $I_{\mathrm{PI}} \in \mathbb{R}$. Further, the computed compressor speed is limited between the minimum and maximum speeds $n_{\mathrm{cpr}}^{\mathrm{min}}$ and $n_{\mathrm{cpr}}^{\mathrm{max}}$, respectively.

The parameters of the rule-based PI controller are listed in Table 3. The PI controller gains were tuned using the the Matlab PID Tuner application [40] to obtain a closed-loop bandwidth of 0.01 rad/s and 10° phase margin.

Table 3. Parameters of rule-based PI controller.

Parameter	Value
T_s	20s
n_{cpr}^{min}	700 rpm
n_{cpr}^{max}	5000 rpm
N^{up}, N^{down}	5
ϑ_{cc}^{ref}	5 °C
H_ϑ	0.4 °C
P_{PI}	−764
I_{PI}	−16.2

5. Simulation Setup

A simulation-based approach was used to study the refrigeration system's performance with differently sized secondary loop storage capacities, a methodology frequently used in the literature to design other cooling systems [12–14]. Matlab/Simulink [41] was used as the simulation environment, where the continuous-time model described in Section 2 and the discrete-time controllers are simulated in a closed loop. The parameters of the simulation study and the individual simulations are given in Table 4.

Table 4. Parameters of simulation study and individual simulations.

Condition	Value
Simulation study:	
K_{sl}^{scl}	$\{0.125, 0.25, 0.375, 0.5, 0.625, 0.75, 0.875, 1, 1.125, \ldots$ $1.25, 1.375, 1.5, 1.75, 2, 2.25, 2.5, 3, 3.5, 4\}$
# of scaling factors	19
# of door opening realizations	7
# of controllers	2
# of simulations	$19 \cdot 7 \cdot 2 = 266$
Individual simulation:	
T_{sim}	120 min
ϑ_{amb}	22 °C
Door openings:	
Start	$[20\text{ min} + \omega_1, 45\text{ min} + \omega_2, 70\text{ min} + \omega_3, 90\text{ min} + \omega_4]$
Duration	[3 min, 1 min, 4 min, 2 min]
$T2TW^{max}$	[100 s, 60 s, 120 s, 80 s]
Initial conditions:	
x_c	$[2.70\text{ °C}, 5\text{ °C}, 5.27\text{ °C}, 6.69\text{ °C}]^T$
u_c	1080 rpm
m	7
Computation:	
Processor	Intel Core i9-10850K [42]
RAM	32 GB
Solver	Matlab ode15s [43]

A total of 19 differently sized storage loops were examined by varying the scaling factors K_{sl}^{scl} between 0.125 and 4. Each storage loop size is simulated seven times with different disturbances due to door openings, for both the MPC and the rule-based PI controller. This results in 266 individual simulations.

Each simulation has a length of $T_{sim} = 120$ min. Within this period, the system is disturbed by four door openings, lasting between 1 and 4 min. Because the timings of these switching disturbances strongly influence the results, the starting time of each of the door openings is randomly shifted by $\omega_{1,2,3,4} \in \mathbb{R}$, normally distributed random numbers in the

interval $(-125\,\text{s}, 125\,\text{s})$. These random door opening shifts are generated seven times for each of the simulations with the same secondary loop sizing and controller (values listed in Appendix C). In this manner, the controllers and the differently sized storage loops are evaluated with the same seven different door opening timings.

Logistics information systems are widely used in the industry for route planning for refrigerated vehicles. These systems also provide information about the time of door openings, when cargo is loaded or unloaded. In this work, it is assumed that these timings are perfectly accurate. Hence, the door openings in the simulation are precisely embedded in the MPC predictions of disturbances. Furthermore, the profile of the temperature window is derived from those predicted door openings. The temperature window is inactive during the duration of the door openings and the period $\text{T2TW}^{\max} \in \mathbb{R}_{\geq 0}$ after the door is closed. Further, it is assumed that the full state measurement or state reconstruction is available without uncertainty or measurement noise for this simulation study.

Each simulation starts at a steady state, where the cooling chamber temperature equals the reference temperature $\vartheta_{\text{cc}}^{\text{ref}}$, and the cooling unit and fan are active with a closed door. The ambient temperature is 22 °C for all simulations, which corresponds to the year-round temperatures in Central Europe for which the vehicle under consideration was configured. Furthermore, the adopted model [28] was identified at similar ambient temperatures and thus is most accurate in this outside temperature range.

6. Results

In this section, the results of the simulation study are presented. First, the MPC and the rule-based PI controller are compared using two simulations with equally sized secondary loops. Then, the results of all simulations are statistically evaluated, and the optimal storage loop sizing is determined.

6.1. Controller Evaluation

Figure 4 shows the results of two exemplary simulations with the same secondary loop sizing.

The two uppermost graphs show the simulated temperatures of the cooling chamber and the thermal energy storage. Below, the power consumption of the compressor, the condenser fan and glycol pump, and the air chiller fan are displayed, allowing to conclude on the respective control variables selected by the controllers. Both controllers hold the cooling chamber temperature during steady-state operation without door openings inside the temperature window, marked in blue. However, after the door openings, indicated by the orange background shading, the MPC can cool down the cooling chamber significantly faster than the rule-based PI controller. Before the door openings, the MPC increases the compressor speed but does not activate the air chiller fan. As a result, thermal energy is stored in the secondary loop, lowering the glycol temperature. When the door is closed again, the MPC activates the air chiller fan and cools the cooling chamber quickly due to the large temperature difference between the glycol and the air inside the cooling chamber. The rule-based PI controller lacks information about future door openings and thus does not react in advance.

A difference between the two controllers is also evident in the energy consumption, $E_{\text{con}} \in \mathbb{R}_{\geq 0}$, which can be derived from the power consumption according to

$$E_{\text{con}} = \int_0^{T_{\text{sim}}} P_{\text{tot}}(t; m)\, dt. \tag{36}$$

In the simulation shown in Figure 4, the MPC consumes 693 Wh, and the rule-based PI controller 795 Wh. The power consumption graphs also indicate that the most energy consumption is attributable to door openings. Stationary operation with a closed door requires significantly less power due to the good insulation of the walls. Furthermore, the computational time of the closed-loop simulation with the MPC is significantly longer than with the rule-based PI controller due to the complexity of the optimization task. In fact, the

single simulation with the MPC takes 62.7 min, while with the rule-based PI controller, it only takes 3.24 s.

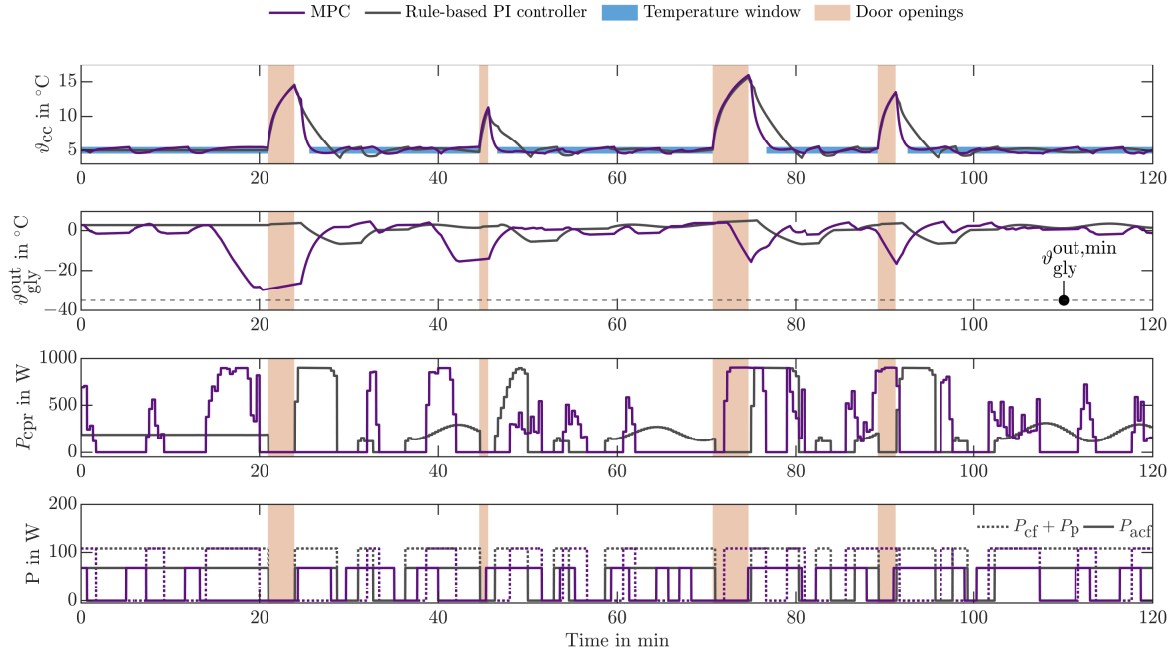

Figure 4. Closed-loop simulation results with MPC and rule-based PI controller with $K_{sl}^{scl} = 1$ and $\omega_1 = 55.1$ s, $\omega_2 = -25.8$ s, $\omega_3 = 42.6$ s, and $\omega_4 = -46.6$ s. The 4 door openings are indicated by an orange background shading, and the MPC temperature window by a blue background shading. The two upper diagrams depict the air temperature inside the cooling chamber and the glycol temperature with the MPC and rule-based PI controller. The lower two diagrams show the power consumption of the components, from which the control variables for the compressor speed, cooling unit status, and air chiller fan status can be derived.

6.2. Simulation Study

For the statistical evaluation of the simulations, two performance parameters are introduced to improve the comparability of the results. The energy consumption of each simulation is related by $\lambda_{con} \in \mathbb{R}_{\geq 0}$ to the reference energy consumption according to

$$\lambda_{con} = \frac{E_{con}}{E_{con}^{ref}}, \tag{37}$$

where $E_{con}^{ref} \in \mathbb{R}_{\geq 0}$ is the mean energy consumption of the seven simulations with the MPC and $K_{sl}^{scl} = 1$.

The relative time to reach the target temperature after door openings $\lambda_{t2tw} \in \mathbb{R}_{\geq 0}$ is defined according to

$$\lambda_{t2tw} = \frac{\mathrm{T2TW}}{\mathrm{T2TW}^{max}}, \tag{38}$$

where $\mathrm{T2TW} \in \mathbb{R}_{\geq 0}$ is the time to reach the upper bound of the temperature window ϑ_{tw}^{max} after each door opening.

Additionally, the scaling factor of the storage loop was generalized to make the results of this work applicable to cooling chambers with different dimensions by defining the dimensionless relative thermal storage capacity of the secondary loop, $\lambda_{cap} \in \mathbb{R}_{\geq 0}$, given by

$$\lambda_{cap}(K_{sl}^{scl}) = \frac{C_{gly}^{scl}(K_{sl}^{scl})}{C_{cc}}, \tag{39}$$

where $C_{\text{gly}}^{\text{scl}} = K_{\text{sl}}^{\text{scl}} C_{\text{gly}} \in \mathbb{R}_{\geq 0}$ is the scaled storage capacity of the glycol loop, and $C_{\text{cc}} = \xi_1^{-1} \in \mathbb{R}_{\geq 0}$ the thermal capacity of the air inside the cooling chamber with the model parameter $\xi_1 \in \mathbb{R}$ (value, see Appendix A).

Figure 5 shows the two performance parameters for each simulation depending on the relative capacity of the storage loop. A line and background shading highlight the mean and standard deviation of the simulations for each relative thermal storage capacity.

For both controllers, the energy consumption decreases as the storage capacity of the secondary loop increases. However, the energy consumption of the rule-based PI controller is generally around 20% higher compared with the MPC. Further, the relative time for reaching the temperature window increases with increasing the storage capacity of the glycol loop. As shown in the individual simulations above, the rule-based PI controller takes about twice as long to cool down the cooling chamber after a door opening compared with the MPC. Furthermore, at very small thermal storage capacities of the secondary loop, the power consumption and the time to reach the temperature window increase significantly with the MPC. In fact, the energy consumption is around 20% higher compared with the slightly larger storage capacities with the same controller.

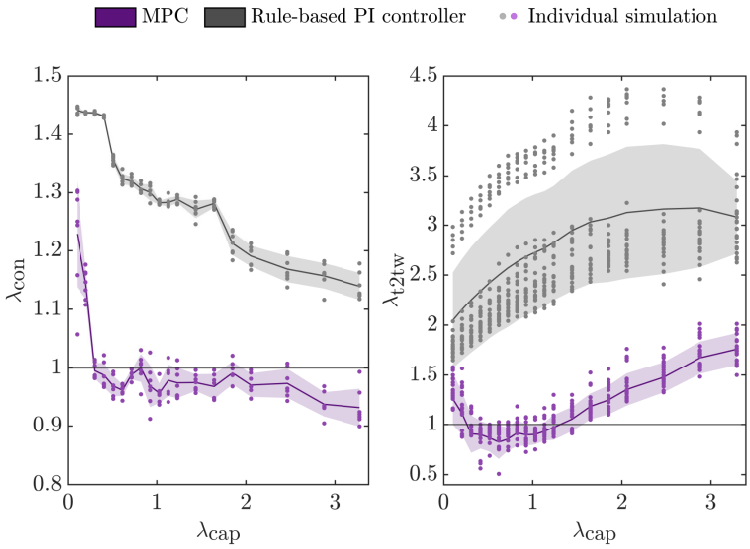

Figure 5. Simulation results of the relative energy consumption λ_{con} and relative time for reaching the target temperature after door openings λ_{t2tw} for different relative secondary loop thermal capacities λ_{cap} with the MPC and the rule-based PI controller. The mean and standard deviation of the simulations for each thermal storage capacity and controller are highlighted by a line and background shading, respectively.

The amplitude statistic of the glycol temperature for different storage capacities is shown in Figure 6.

With the MPC, the glycol temperature is much lower at small thermal storage capacities and spans a broader temperature range. Moreover, the system is more affected by the minimum glycol temperature at low thermal storage capacities. However, with the rule-based PI controller, the glycol temperature remains relatively constant over the entire λ_{cap} range and has a small variance. This also shows that this conventional temperature controller cannot utilize the thermal energy storage due to its simple heuristic control law in which the cooling unit and fan are operated in parallel.

To facilitate the sizing of the secondary loop storage capacity, the parameter $\lambda_{\text{per}} \in \mathbb{R}_{\geq 0}$ is introduced, which gives the controller performance according to

$$\lambda_{\text{per}} = \psi \, \bar{\lambda}_{\text{con}} + (1 - \psi) \, \bar{\lambda}_{\text{t2tw}}, \tag{40}$$

where $\bar{\lambda}_{\text{con}} \in \mathbb{R}_{\geq 0}$ and $\bar{\lambda}_{\text{t2tw}} \in \mathbb{R}_{\geq 0}$ are the means of λ_{con} and λ_{t2tw} for the different secondary loop storage capacities of the individual simulations, and $\psi \in \mathbb{R}_{\geq 0}$ is a weighting factor between 0 and 1. The weighting factor can either prioritize low energy consumption or fast cooling after door openings in the secondary loop storage capacity design. Figure 7 shows λ_{per} for three different weighting factors and indicates the optimal sizing of the secondary loop with the MPC.

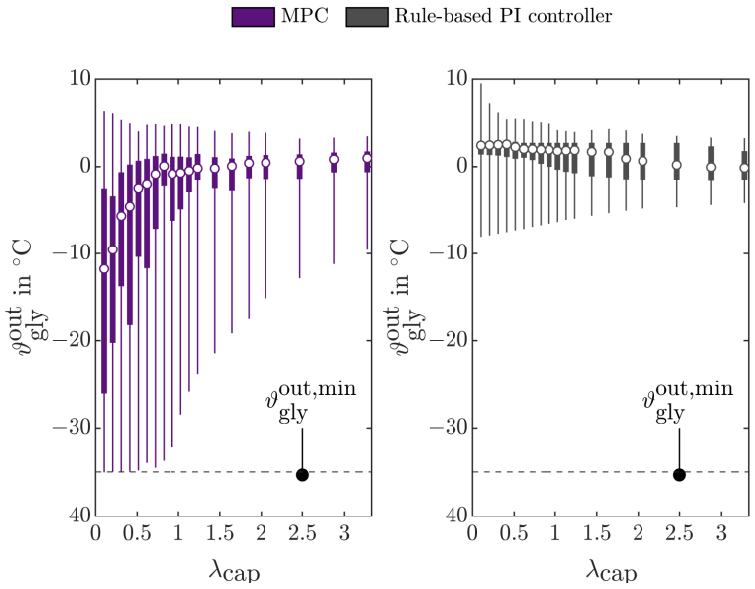

Figure 6. Amplitude statistic of glycol temperature $\vartheta^{\text{out}}_{\text{gly}}$ plotted for the different relative thermal storage capacities with the MPC and rule-based PI controller. A circle indicates the mean glycol temperatures for each secondary loop storage size, and a dashed line highlights the minimum permissible glycol temperature $\vartheta^{\text{out,min}}_{\text{gly}}$.

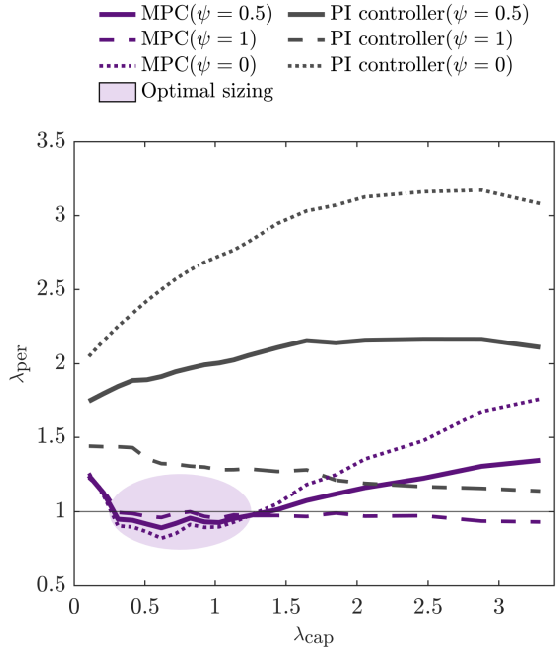

Figure 7. Controller performance λ_{per} for three different weighting factors ψ depending on the relative storage capacity of the secondary loop λ_{cap}. Control performance is defined with $\psi = 1$ solely by the relative energy consumption λ_{con}, with $\psi = 0$ by the relative time to reach the temperature window after door openings λ_{t2tw}, and with $\psi = 0.5$ by equally weighting λ_{con} and λ_{t2tw}. A region of an optimal relative secondary loop storage capacity can be observed for the MPC, where both the minimum energy consumption and fast cooling after door openings are realized.

With $\psi = 1$, the design exclusively focuses on minimal energy consumption, while for $\psi = 0$, only the time to reach the temperature window after door openings is considered. When both targets should be equally satisfied, with $\psi = 0.5$, a clear optimum between $\lambda_{\text{cap}} = 0.25$ and $\lambda_{\text{cap}} = 1.25$ is observable for the MPC. The rule-based PI controller performs much worse than the MPC, and no obvious optimum exists. Therefore, the design can either focus on fast cooling after door openings with high energy consumption or vice versa.

7. Discussion

The thermal storage capacity of the storage loop must be chosen appropriately, as both an over- and undersized secondary loop can hinder the overall performance of the cooling system. Employing an MPC, an undersized storage loop increases energy consumption and reduces the temperature control capability due to the limitations of the minimum glycol temperature, which only allows an insufficient amount of thermal energy to be stored in the secondary loop for the given cooling chamber. With an oversized secondary loop, the pass-through of the control input to the cooling chamber temperature gets too slow. Due to the finite horizon of the MPC, caused by limited computational resources, the time before door openings is too short to cool down the storage loop sufficiently to achieve fast cooling after door openings. On the other hand, the rule-based PI controller is unsuitable for utilizing the thermal storage of the secondary loop and thus has significantly higher energy consumption and takes longer to cool down the cooling chamber after door openings, which is in line with [22,29]. From the results, it is also evident that a smaller storage capacity leads to greater agility of the system since the pass-through of the controlled variables on the temperature inside the cooling chamber is faster, as also stated in [23]. This allows the controller to respond quickly to incorrectly predicted door openings, model errors, or other disturbances.

Overall, this work shows the importance of considering the control strategy besides the vehicle operating conditions, such as ambient temperature, door openings, or other exogenous factors, when sizing the secondary loop storage capacity for the implementation in real-world refrigerated vehicles. Furthermore, this work recommends using predictive controllers for temperature control of secondary loop cooling systems, as only those are suitable to utilize the thermal energy storage of the secondary loop by predicting the future required cooling capacity.

However, the proposed sizing concept for the secondary loop storage capacity comes at the expense of extensive closed-loop simulations. Especially with the MPC, the computational time is substantial due to the complexity of the optimization task, even though, for example, limited horizon length and move blocking were applied. Although it is not a problem for the offline simulations performed, both controllers are real-time capable and thus suitable for application in actual refrigerated vehicles, which was also experimentally shown for similar control schemes in [29,44].

Since the vehicle under consideration is intended for use in Central Europe, simulations with an ambient temperature of 22 °C, characteristic for this region of the world, are considered in this work. Nevertheless, the proposed methodology offers the possibility to consider different ambient temperatures to adapt the sizing of the secondary loop thermal capacity to the specific operating conditions under which the vehicle shall be operated. However, for ambient temperatures below the freezing point, it is recommended to extend the model of the refrigerated vehicle to account for ice formation and mass infiltration during door openings as discussed in [28].

Furthermore, when designing a refrigeration system, one should consider economic factors, as was done in [11,12,45,46]. The costs of the refrigeration system over its entire lifetime are mainly driven by its energy consumption when considering a fixed system architecture (secondary loop cooling system with a sensible heat medium). A change in the thermal storage capacity of the secondary loop and the associated change in the amount of

glycol only marginally affects the costs. Hence, energy consumption was the only economic factor considered when optimizing the secondary loop storage capacity.

By expanding the model with a submodel for the cargo as described by [47,48], the thermal capacity of the cargo could be considered in the optimization of the secondary loop sizing. However, as is common for small-scale refrigerated vehicles, the frequent change of different types of cargo, whose parameters are often unknown, makes this approach impractical. Therefore, an empty cooling chamber was assumed in this work, which is the most conservative approach, as there is no additional thermal storage within the cooling chamber.

The proposed sizing concept can be utilized to design secondary loop refrigeration systems, increasing their efficiency and cooling performance. In addition, optimizing the sizing of the secondary loop can allow for a smaller cooling unit design, which further entails increased efficiency and lifetime, and reduces the acquisition costs of the cooling system. In general, combining a secondary loop refrigeration system with a suitable control scheme can be a simple alternative to more complex and costly cooling systems with PCM-based TES [14,22].

Future work includes the consideration of the vehicle's powertrain when optimizing the size of the refrigeration system's thermal energy storage. Since in most refrigerated vehicles, the energy for the cooling system is provided directly by the vehicle's powertrain, optimizing the thermal energy storage of the refrigeration system can enable the use of load-shifting strategies for the powertrain to increase the vehicle's energy efficiency further. Another task of interest is optimizing the cooling power of the primary loop in parallel to the size of the thermal energy storage.

8. Conclusions

This work studies the parameter of the storage capacity of a secondary loop cooling unit for a small-scale refrigerated vehicle. By closed-loop simulations of an experimentally validated refrigerated vehicle model, a mixed-integer MPC and a rule-based PI controller are evaluated with different thermal storage capacities of the secondary loop. The results show that the predictive control concept with a suitable secondary loop storage capacity can save energy and increase the cooling performance in the event of door openings. For the MPC, the optimal thermal storage capacity of the secondary loop is between 0.25 and 1.25 times the thermal capacity of the air inside the cooling chamber. At this size, both minimum energy consumption and fast cooling after door openings are equally met. In particular, the energy savings of up to 20% compared to an undersized thermal energy storage system are very promising for reducing the environmental impact of refrigerated vehicles. Since future door openings are not explicitly considered in the control law, the conventional rule-based PI controller cannot exploit the advantages of the storage capability of the secondary loop and performs significantly worse than the predictive controller. With the rule-based PI controller, minimum energy consumption and rapid cooling after door openings conflict, and no clear optimum can be found for both goals. Therefore, this work shows that only an appropriately sized secondary loop, in combination with a suitable control concept, can exploit the full potential of secondary loop refrigeration systems. Thus, it is of great importance that the design of the cooling system takes into account not only the operating conditions of the vehicle but also the control strategy.

Author Contributions: Conceptualization and methodology, M.L., M.F., A.P. and M.K.; investigation and validation, M.L. and M.F.; data curation, M.L.; software and visualization, M.L; writing—original draft preparation, M.L.; writing—review and editing, M.F., A.P. and M.K.; resources, supervision, project administration and funding acquisition, M.K. All authors have read and agreed to the published version of the manuscript.

Funding: This research was funded by the Austrian Research Promotion Agency (Forschungsforderungsgesellschaft) by the project ZETA [grant number 891917].

Data Availability Statement: Confidentiality agreements do not allow the publication of the data presented in this study.

Acknowledgments: The authors acknowledge TU Wien Bibliothek for financial support through its Open Access Funding Programme.

Conflicts of Interest: The authors declare no conflict of interest.

Abbreviations

The following abbreviations are used in this manuscript:

MPC	Model predictive controller
PCM	Phase change material
PI	Proportional–integral
TES	Thermal energy storage

Appendix A. State-Space Representation of Hybrid Model

Matrices appearing in the state-space representation of the model (1)–(2):

$$\boldsymbol{A}(m) = \begin{bmatrix} A_{11}(m) & A_{12}(m) & \xi_2 & 0 \\ \chi_3\, R_1(m) & A_{22}(m) & 0 & 0 \\ \zeta_1 & 0 & -(\zeta_1+\zeta_2) & \zeta_2 \\ 0 & 0 & \zeta_3 & -(\zeta_3+\zeta_4) \end{bmatrix}$$

$$\boldsymbol{B}(m) = \begin{bmatrix} -\alpha_1\chi_1\xi_1\, R_1(m)\, s_{\mathrm{cu}}(t) \\ -\alpha_1\chi_1\,[\chi_2 - \chi_3\, R_1(m)]\, s_{\mathrm{cu}}(t) \\ 0 \\ 0 \end{bmatrix}$$

$$\boldsymbol{E}(m) = \begin{bmatrix} \xi_3\, s_{\mathrm{door}}(t) + \alpha_2\chi_1\xi_1\, R_1(m)\, s_{\mathrm{cu}}(t) \\ \alpha_2\chi_1\,[\chi_2 - \chi_3\, R_1(m)]\, s_{\mathrm{cu}}(t) \\ 0 \\ \zeta_4 \end{bmatrix}$$

$$\boldsymbol{g}(m) = \begin{bmatrix} \xi_1\,[\alpha_4\chi_1\, R_1(m) + R_3(m)]\, s_{\mathrm{cu}}(t) + \xi_1\kappa_1\, s_{\mathrm{acf}}(t) \\ \alpha_4\chi_1\,[\chi_2 - \chi_3\, R_1(m)]\, s_{\mathrm{cu}}(t) \\ 0 \\ 0 \end{bmatrix}$$

$$\boldsymbol{C}(m) = \begin{bmatrix} 1 & 0 & 0 & 0 \\ 0 & 1-\alpha_3\,\chi_1\, s_{\mathrm{cu}}(t) & 0 & 0 \\ 0 & 1 & 0 & 0 \\ \kappa_6\, s_{\mathrm{cu}}(t) & 0 & 0 & 0 \\ \kappa_6\, s_{\mathrm{cu}}(t) & 0 & 0 & 0 \\ 0 & 0 & 0 & 0 \\ 0 & 0 & 0 & 0 \\ 0 & 0 & 0 & 0 \end{bmatrix} \qquad \boldsymbol{D}(m) = \begin{bmatrix} 0 \\ 0 \\ 0 \\ \kappa_4\, s_{\mathrm{cu}}(t) \\ \kappa_4\, s_{\mathrm{cu}}(t) \\ 0 \\ 0 \\ 0 \end{bmatrix}$$

$$\boldsymbol{F}(m) = \begin{bmatrix} 0 \\ 0 \\ 0 \\ \kappa_5\, s_{\mathrm{cu}}(t) \\ \kappa_5\, s_{\mathrm{cu}}(t) \\ 0 \\ 0 \\ 0 \end{bmatrix} \qquad \boldsymbol{h}(m) = \begin{bmatrix} 0 \\ 0 \\ 0 \\ \kappa_1\, s_{\mathrm{acf}}(t) + (\kappa_2+\kappa_3-\kappa_7)\, s_{\mathrm{cu}}(t) \\ -\kappa_7\, s_{\mathrm{cu}}(t) \\ \kappa_2\, s_{\mathrm{cu}}(t) \\ \kappa_3\, s_{\mathrm{cu}}(t) \\ \kappa_1\, s_{\mathrm{acf}}(t) \end{bmatrix}$$

with

$$A_{11}(m) = -\xi_2 - \xi_3\, s_{\text{door}}(t) - \xi_1\,[R_1(m) - R_2(m)\, s_{\text{cu}}(t)] \tag{A1}$$
$$A_{12}(m) = \xi_1\, R_1(m)\,[1 - \alpha_3 \chi_1\, s_{\text{cu}}(t)] \tag{A2}$$
$$A_{22}(m) = \alpha_3\, \chi_1\,[-\chi_2 - \chi_3\, R_1(m)]\, s_{\text{cu}}(t) - \chi_3\, R_1(m) \tag{A3}$$

and

$$R_1(m) := \beta_1\, s_{\text{acf}}(t) + \beta_2\,[1 - s_{\text{acf}}(t)] \tag{A4}$$
$$R_2(m) := -\gamma_1\, s_{\text{acf}}(t) + \gamma_3\,[1 - s_{\text{acf}}(t)] \tag{A5}$$
$$R_3(m) := \gamma_2\, s_{\text{acf}}(t) + \gamma_4\,[1 - s_{\text{acf}}(t)] \tag{A6}$$

The parameter values of the model are listed in Table A1.

Table A1. Model parameter values (adopted from [28]).

Parameter	Value	Unit
α_1	$9.24 \cdot 10^{-5}$	$\mathrm{W\,rpm^{-1}}$
α_2	$6.78 \cdot 10^{-4}$	$\mathrm{W(^\circ C)^{-1}}$
α_3	$4.25 \cdot 10^{-3}$	$\mathrm{W(^\circ C)^{-1}}$
α_4	$2.85 \cdot 10^{-2}$	W
β_1	$1.40 \cdot 10^{2}$	$\mathrm{W\,K^{-1}}$
β_2	4.46	$\mathrm{W\,K^{-1}}$
γ_1	34.3	$\mathrm{W(^\circ C)^{-1}}$
γ_2	$2.93 \cdot 10^{2}$	W
γ_3	10.2	$\mathrm{W(^\circ C)^{-1}}$
γ_4	0	W
κ_1	68.5	W
κ_2	65.0	W
κ_3	43.2	W
κ_4	0.178	$\mathrm{W\,rpm^{-1}}$
κ_5	10.1	$\mathrm{W(^\circ C)^{-1}}$
κ_6	0.510	$\mathrm{W(^\circ C)^{-1}}$
κ_7	$2.28 \cdot 10^{2}$	W
χ_1	$2 \cdot 10^{-2}$	$\mathrm{K\,W^{-1}}$
χ_2	17.5	$\mathrm{s^{-1}}$
χ_3	$7.42 \cdot 10^{-5}$	$\mathrm{K(W\,s)^{-1}}$
ξ_1	$6.09 \cdot 10^{-5}$	$\mathrm{K(W\,s)^{-1}}$
ξ_2	$2.96 \cdot 10^{-2}$	$\mathrm{s^{-1}}$
ξ_3	$1.39 \cdot 10^{-2}$	$\mathrm{s^{-1}}$
ζ_1	$1.42 \cdot 10^{-2}$	$\mathrm{s^{-1}}$
ζ_2	$2.67 \cdot 10^{-3}$	$\mathrm{s^{-1}}$
ζ_3	$1.18 \cdot 10^{-3}$	$\mathrm{s^{-1}}$
ζ_4	$1.10 \cdot 10^{-4}$	$\mathrm{s^{-1}}$

Appendix B. Blocking Matrix

Table A2 lists each of the 30 non-zero elements of the blocking matrix T_{mb}, given by the row number R, column number C, and value V.

Table A2. Non-zero entries of the move blocking matrix T_{mb}, given by its row number R, column number C, and value V.

R	1	2	3	4	5	6	7	8	9	10
C	1	2	3	4	5	6	7	8	9	10
V	1	1	1	1	1	1	1	1	1	1
R	11	12	13	14	15	16	17	18	19	20
C	11	11	11	11	11	12	12	12	12	12
V	1	1	1	1	1	1	1	1	1	1
R	21	22	23	24	25	26	27	28	29	30
C	13	13	13	13	13	13	13	13	13	13
V	1	1	1	1	1	1	1	1	1	1

Appendix C. Door-Opening Shifts

The seven sets of randomly generated shifts of door openings are listed in Table A3.

Table A3. Values of the 7 sets of door-opening shifts.

Nr.	ω_1	ω_2	ω_3	ω_4
1	55.1 s	−25.8 s	42.6 s	−46.6 s
2	−20.7 s	−38.6 s	−118 s	117 s
3	−125 s	9.70 s	−20.7 s	48.1 s
4	−49.4 s	−20.2 s	14.7 s	94.1 s
5	−88.3 s	46.3 s	−89.9 s	98.7 s
6	−102 s	−73.9 s	−75.5 s	−104 s
7	−78.4 s	94.5 s	75.2 s	−115 s

References

1. Han, J.W.; Zhao, C.J.; Qian, J.P.; Ruiz-Garcia, L.; Zhang, X. Numerical modeling of forced-air cooling of palletized apple: Integral evaluation of cooling efficiency. *Int. J. Refrig.* **2018**, *89*, 131–141. [CrossRef]
2. Tassou, S.; De-Lille, G.; Ge, Y. Food transport refrigeration—Approaches to reduce energy consumption and environmental impacts of road transport. *Appl. Therm. Eng.* **2009**, *29*, 1467–1477. [CrossRef]
3. Tassou, S.; Lewis, J.; Ge, Y.; Hadawey, A.; Chaer, I. A review of emerging technologies for food refrigeration applications. *Appl. Therm. Eng.* **2010**, *30*, 263–276. [CrossRef]
4. Maiorino, A.; Petruzziello, F.; Aprea, C. Refrigerated Transport: State of the Art, Technical Issues, Innovations and Challenges for Sustainability. *Energies* **2021**, *14*, 7237. [CrossRef]
5. James, S.; James, C.; Evans, J. Modelling of food transportation systems—A review. *Int. J. Refrig.* **2006**, *29*, 947–957.
6. Maiorino, A.; Mota-Babiloni, A.; Petruzziello, F.; Del Duca, M.G.; Ariano, A.; Aprea, C. A Comprehensive Energy Model for an Optimal Design of a Hybrid Refrigerated Van. *Energies* **2022**, *15*, 4864. [CrossRef]
7. Stoecker, W.; Jones, J. *Refrigeration and Air Conditioning*; Mc GrawHill Book Co.: New York, NY, USA, 1982.
8. Artuso, P.; Rossetti, A.; Minetto, S.; Marinetti, S.; Moro, L.; Col, D.D. Dynamic modeling and thermal performance analysis of a refrigerated truck body during operation. *Int. J. Refrig.* **2019**, *99*, 288–299. [CrossRef]
9. Sun, Y.; Gu, L.; Wu, C.J.; Augenbroe, G. Exploring HVAC system sizing under uncertainty. *Energy Build.* **2014**, *81*, 243–252. [CrossRef]
10. Djunaedy, E.; van den Wymelenberg, K.; Acker, B.; Thimmana, H. Oversizing of HVAC system: Signatures and penalties. *Energy Build.* **2011**, *43*, 468–475. [CrossRef]
11. Khosravi, A.; Koury, R.; Machado, L. Thermo-economic analysis and sizing of the components of an ejector expansion refrigeration system. *Int. J. Refrig.* **2018**, *86*, 463–479. [CrossRef]
12. Negrão, C.O.; Hermes, C.J. Energy and cost savings in household refrigerating appliances: A simulation-based design approach. *Appl. Energy* **2011**, *88*, 3051–3060. [CrossRef]
13. Hermes, C.J.; Melo, C.; Knabben, F.T.; Gonçalves, J.M. Prediction of the energy consumption of household refrigerators and freezers via steady-state simulation. *Appl. Energy* **2009**, *86*, 1311–1319. [CrossRef]
14. Fasl, J. Modeling and Control of Hybrid Vapor Compression Cycles. Master's Thesis, University of Illinois at Urbana-Champaign, Champaign, IL, USA, 2013.
15. Huang, Y.; Khajepour, A.; Khazraee, M.; Bahrami, M. A Comparative Study of the Energy-Saving Controllers for Automotive Air-Conditioning/Refrigeration Systems. *J. Dyn. Syst. Meas. Control* **2016**, *139*, 014504. [CrossRef]
16. Alva, G.; Lin, Y.; Fang, G. An overview of thermal energy storage systems. *Energy* **2018**, *144*, 341–378. [CrossRef]

17. Wang, N.; Tang, J.; Shan, H.S.; Jia, H.Z.; Peng, R.L.; Zuo, L. Efficient Power Conversion Using a PV-PCM-TE System Based on a Long Time Delay Phase Change With Concentrating Heat. *IEEE Trans. Power Electron.* **2023**, *38*, 10729–10738. [CrossRef]
18. Ilangovan, A.; Hamdane, S.; Silva, P.D.; Gaspar, P.D.; Pires, L. Promising and Potential Applications of Phase Change Materials in the Cold Chain: A Systematic Review. *Energies* **2022**, *15*, 7683. [CrossRef]
19. Bakhshipour, S.; Valipour, M.; Pahamli, Y. Parametric analysis of domestic refrigerators using PCM heat exchanger. *Int. J. Refrig.* **2017**, *83*, 1–13. [CrossRef]
20. Jeong, S.; Jang, K.; Ko, J. A novel concept of rapid cooling method of refrigeration system. *Int. J. Refrig.* **2005**, *28*, 176–182. [CrossRef]
21. Mousazade, A.; Rafee, R.; Valipour, M.S. Thermal performance of cold panels with phase change materials in a refrigerated truck. *Int. J. Refrig.* **2020**, *120*, 119–126. [CrossRef]
22. Shafiei, S.E.; Alleyne, A. Model predictive control of hybrid thermal energy systems in transport refrigeration. *Appl. Therm. Eng.* **2015**, *82*, 264–280. [CrossRef]
23. Wang, K.; Eisele, M.; Hwang, Y.; Radermacher, R. Review of secondary loop refrigeration systems. *Int. J. Refrig.* **2010**, *33*, 212–234. [CrossRef]
24. Bhattad, A.; Sarkar, J.; Ghosh, P. Exergetic analysis of plate evaporator using hybrid nanofluids as secondary refrigerant for low-temperature applications. *Int. J. Exergy* **2017**, *24*, 1–20. [CrossRef]
25. Yi, W.B.; Choi, K.H.; Yoon, J.I.; Son, C.H.; Ha, S.J.; Jeon, M.J. Exergy characteristics of R404A indirect refrigeration system using CO 2 as a secondary refrigerant. *Heat Mass Transf.* **2019**, *55*, 1133–1142. [CrossRef]
26. Vasile, V.; Necula, H.; Badea, A.; Revellin, R.; Bonjour, J.; Haberschill, P. Experimental study of the heat transfer characteristics of a paraffin-in-water emulsion used as a secondary refrigerant. *Int. J. Refrig.* **2018**, *88*, 1–7. [CrossRef]
27. Irsyad, M.; Suwono, A.; Indartono, Y.S.; Pasek, A.D.; Pradipta, M.A. Phase change materials development from salt hydrate for application as secondary refrigerant in air-conditioning systems. *Sci. Technol. Built Environ.* **2018**, *24*, 90–96. [CrossRef]
28. Fallmann, M.; Poks, A.; Kozek, M. Control-oriented hybrid model of a small-scale refrigerated truck chamber. *Appl. Therm. Eng.* **2023**, *220*, 119719. [CrossRef]
29. Lösch, M. Design, Implementation, and Experimental Validation of a Model Predictive Control Scheme for a Small-Scale Refrigerated Truck. Master's Thesis, Technische Universität Wien, Vienna, Austria, 2022.
30. *ISO 80000-5:2019*; Quantities and Units—Part 5: Thermodynamics. ISO: Geneva, Switzerland, 2019.
31. PRODUCTBLOKS GmbH. Product Information: Ecos M24. Available online: https://pbx.at/de/products/ (accessed on 8 April 2023).
32. Borrelli, F.; Bemporad, A.; Morari, M. *Predictive Control for Linear and Hybrid Systems*; Cambridge University Press: Cambridge, UK, 2017. [CrossRef]
33. Kumar, S. *Thermal Engineering Volume 1*, 1st ed.; Springer International Publishing: Cham, Switzerland, 2022.
34. Mayer, B.; Killian, M.; Kozek, M. Management of hybrid energy supply systems in buildings using mixed-integer model predictive control. *Energy Convers. Manag.* **2015**, *98*, 470–483. [CrossRef]
35. Cagienard, R.; Grieder, P.; Kerrigan, E.; Morari, M. Move blocking strategies in receding horizon control. *J. Process Control* **2007**, *17*, 563–570. [CrossRef]
36. Wang, L. *Model Predictive Control System Design and Implementation Using MATLAB®*; Springer Science & Business Media: New York, NY, USA, 2009.
37. Löfberg, J. YALMIP: A Toolbox for Modeling and Optimization in MATLAB. In Proceedings of the 2004 IEEE International Conference on Robotics and Automation (IEEE Cat. No.04CH37508), Taipei, Taiwan, 2–4 September 2004.
38. Gurobi Optimization, LLC. *Gurobi Optimizer Reference Manual*; Gurobi Optimization, LLC: Beaverton, OR, USA, 2022.
39. Lunze, J. *Regelungstechnik 2*; Springer: Berlin/Heidelberg, Germany, 2005; Volume 6.
40. MATLAB Control System Toolbox. Available online: https://de.mathworks.com/products/control.html (accessed on 25 March 2023).
41. MATLAB Version: 9.13.0 (R2022b). Available online: https://www.mathworks.com (accessed on 25 August 2023).
42. Datasheet: i9-10850K. Available online: https://www.intel.com (accessed on 8 February 2023).
43. Shampine, L.F.; Reichelt, M.W. The matlab ode suite. *SIAM J. Sci. Comput.* **1997**, *18*, 1–22. [CrossRef]
44. Fallmann, M.; Lösch, M.; Poks, A.; Kozek, M. Energy-efficient hybrid model predictive control of mobile refrigeration systems. *Appl. Therm. Eng.* **2023**, *235*, 121347. [CrossRef]
45. Yu, M.; Cui, P.; Wang, Y.; Liu, Z.; Zhu, Z.; Yang, S. Advanced Exergy and Exergoeconomic Analysis of Cascade Absorption Refrigeration System Driven by Low-Grade Waste Heat. *ACS Sustain. Chem. Eng.* **2019**, *7*, 16843–16857. [CrossRef]
46. Yu, M.; Chen, Z.; Yao, D.; Zhao, F.; Pan, X.; Liu, X.; Cui, P.; Zhu, Z.; Wang, Y. Energy, exergy, economy analysis and multi-objective optimization of a novel cascade absorption heat transformer driven by low-level waste heat. *Energy Convers. Manag.* **2020**, *221*, 113162. [CrossRef]

47. Luchini, E.; Radler, D.; Ritzberger, D.; Jakubek, S.; Kozek, M. Model predictive temperature control and ageing estimation for an insulated cool box. *Appl. Therm. Eng.* **2018**, *144*, 269–277. [CrossRef]
48. Raval, A.; Solanki, S.; Yadav, R. A simplified heat transfer model for predicting temperature change inside food package kept in cold room. *J. Food Sci. Technol.* **2013**, *50*, 257–265. [CrossRef]